ELSEVIER

Physica D 97 (1996) 311–321

PHYSICA D

Multiple states in doubly driven flow

J.A. Whitehead [1]

Department of Physical Oceanography, MS-21 Woods Hole Oceanographic Institution, Woods Hole, MA 02543-1047 USA

Abstract

It has been known since 1961 that if two components effect density, a convecting fluid may possess multiple stable states for the same boundary conditions. Until recently, analytical and numerical calculations have been conducted for application to climate models. Laboratory observations were absent. Experiments have now produced the anticipated multiple states and also give new insight into their physical nature. A new, wider range of applications to estuary and coastal water circulation is indicated. In the experiments a chamber of water was heated from below and exposed to a constant volume flux of salty water from above. This was connected to a large reservoir of fresh room temperature water through two horizontal tubes, one near the top and the other near the bottom. Parameters were such that the time constant for change of temperature was less than the time constant for change in salinity. The experiments confirmed the principal prediction of theory – that two states can exist for the same boundary conditions. The range of two stable states was mapped as a function of the temperature forcing for fixed salinity flux. For low thermal forcing, the salinity driven state was found. This had very slow exchange of warm and very salty water with the reservoir. Density due to salinity was greater than that from temperature. Above a critical forcing an additional state could exist. This possessed exchange with the reservoir in the opposite direction of warm and much lower salinity water above approximately 1.5 times the critical forcing, only the thermal state was found. A second example driven by stress and heat flux also exhibits multiple states. Two examples are analyzed.

1. Introduction

The pioneering studies of Malkus and Veronis [7], Busse [1], Schluter et al. [8], and Busse [2] showed how both infinitesimal and finite amplitude instability analysis allows a rational analysis of fluid flow structure. Busse's study in particular showed how the famous hexagonal flow pattern was linked to finite amplitude instabilities in Rayleigh–Benard convection near the critical Rayleigh number. The subsequent analyses of stability of finite amplitude rolls provided a method to extend the study of structures over large ranges of parameters. I was privileged to conduct laboratory experiments with Professor Busse to observe and confirm some of the beautiful roll instability modes and to view new bimodal structures predicted by theory. This article describes a recent set of experiments which are first observations of another aspect of convection and finite amplitude instability that began in the early 1960s.

In the ocean a number of boundary effects produce the motion of the water, including wind stress, differential heating, precipitation, and evaporation. Internal factors such as radiant heating and tides also produce flows. For over 30 years, it has been known that combinations of these forcing factors can produce a body with more than one steady and stable physical state. The first, and most well-known example [9], involves the effects of temperature and salinity on a simple

[1] E-mail: jwhitehead@whoi.edu.

PII S0167-2789(96)00146-7

mixed basin that is connected to a second basin by tubes. In that problem, there were two stable fixed points and one unstable fixed point for some range of the forcing parameters. There have since been roughly a dozen studies of such problems, usually with more complicated basins and more states. In addition, multiple states have been predicted for forced convection [10], and in basins forced by surface stress alone [5,6].

Multiple states are not new, they are well known in hydrodynamics. For example, in traditional aerodynamics one state of motion around a wing with lift and one state without lift ("stall") – both with the same forcing parameters – have understandably been the focus of attention for about a century. The problem of stall depends on the details of boundary layer adjustment to the interior flow, a process often called flow separation. This feature also appears to be possessed by the recent examples of multiple states in oceanic model basins forced by wind stress alone. In contrast, for the problems to be discussed here multiple solutions arise from the competition of interior forces. In this way, they are distant relatives to the multiple states for hexagons analyzed by Busse. In the problems discussed in this article, either the salinity or the stress must force a circulation in the opposite direction from the thermal convection.

2. T–S Driving

The case of a container connected to a large basin with two tubes, one at the top and one at the bottom can be formulated rather precisely. It was developed to explore the combined effect of evaporation/precipitation and temperature on circulation of a body of salt water such as the ocean. Numerous analytical and numerical studies of this problem have been conducted since its inception by Stommel [9] as reviewed by Weaver and Hughes [12], Marotzke [14], and Whitehead [15]. Interestingly, no laboratory study or direct observation in nature of this important process has ever apparently been made. In Stommel's model two boxes containing water were connected side-by-side by two horizontal tubes one at the top and one at the bottom. Diffusion through the walls from unchanging salinity and temperature basins produced temperature and salinity changes to well-mixed water in the boxes. One box was subjected to a basin with positive temperature and salinity and the other to exactly the negative values. But salinity diffuses through the walls at a different rate than heat. This produces some important effects which are different from the usual internal effects of double diffusion. The distinguishing fact is that there were three possible states of motion for the same values of reservoir temperature and salinity (at least within a certain range of forcing parameters). One state is characterized by salinity dominating the density difference between basins which propelled water between basins. The second is predominantly temperature driven. Both of these states were linearly stable, so small perturbations to motion decayed in time. The third state was unstable and the system would drift to one of the other states.

We have been able to verify the main predictions of the theory experimentally. The experimental apparatus (Fig. 1) consisted of one $10 \times 10 \times 8$ cm deep watertight Plexiglas "test chamber" (two active boxes are not needed) with 1" thick Styrofoam thermal insulation on the sides and top. The bottom of the box was a copper plate in contact with hot isothermal water whose temperature was varied from experiment to experiment. The top of the water in the box was in contact with a flat horizontal common household sponge. Above the sponge salt water with density 1.0060 g/cm^3 was pumped in by a precision pump at a metered rate of 0.2 cm^3/s. Thus the water in the test chamber was heated from below and subjected to increased salinity from above. Both have the effect of mixing the test chamber water vertically, but temperature will decrease density while salinity flux will increase it. On one side wall of the box were two horizontal tubes. The centerline of one tube was about 2 cm above the other, which was 1 cm above the copper plate. The two tubes allowed convective flow of water between the chamber and a second reservoir at constant temperature and salinity which corresponds to the ocean. Water flows into the chamber through one tube and out the other, the direction depending on the density of the water in the test chamber compared to the density of the reservoir water. The ocean reservoir was

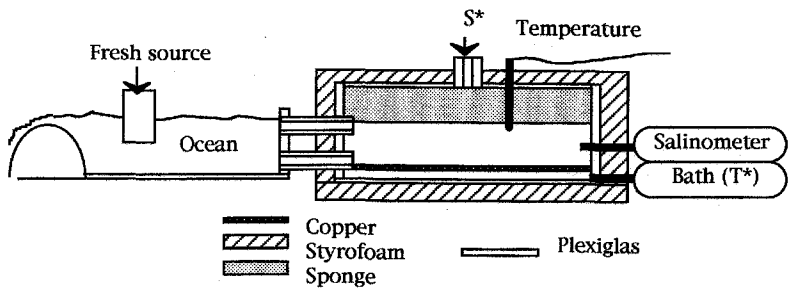

Fig. 1. Sketch of the laboratory apparatus that has shown two states for the same forcing conditions T^* and S^*. A sponge above the water receives a constant flow of water of salinity S^*. The chamber is also heated from below through a metal floor in contact with a bath at temperature T^*. Two tubes connect the chamber to an "ocean" of constant salinity and temperature.

a larger volume of almost completely fresh water kept at room temperature by a thermostatic bath. Fresh water was added to the reservoir at a constant rate of 1–2 cm^3/s. The exposed free top surface of the reservoir was fixed by an overflow out of the ocean so that water depth in the chamber was close to 3 cm. To measure the salinity decay time one stopper was given a small hole to allow outflow of the added volume and recording density response with time for constant T^*. The salinity relaxation time is approximately 1500 s and this agrees with the estimated time V/q. Thermal decay time of the chamber was measured by stopping the exchange flow and recording temperature response with time to a sudden change in T^*. This time constant is about 500 s.

Simple equations for the salinity and temperature (all are deviations from reservoir values) are

$$V\frac{dS}{dt} = qS^* - [|Q| + q]S, \tag{2.1}$$

$$V\rho C_p\frac{dT}{dt} = \frac{kA}{\delta}[T^* - T] - \rho C_p[(|Q| + q)T - qT^*], \tag{2.2}$$

where S^* is the pumped salinity, T^* is temperature of the bath, S, T and V are salinity, temperature and volume within the chamber, respectively, ρ is density C_p is specific heat, Q is volume flux between chamber and reservoir, k is thermal conductivity of the boundary layer above the copper bottom, A is surface area of the chamber bottom, and δ is boundary layer thickness (probably a function of Nusselt number).

These can be rearranged to the more straightforward forms:

$$\frac{dS}{dt} = \frac{1}{\tau_S}[S^* - S] - \frac{|Q|}{V}S \tag{2.3}$$

and

$$\frac{dT}{dt} = \frac{1}{\tau_T}[T^* - T] - \frac{|Q|}{V}T, \tag{2.4}$$

where

$$\tau_S = \frac{V}{q} \quad \text{and} \quad \tau_T = \left[\frac{k}{\delta H\rho C_p} + \frac{q}{V}\right]^{-1} \tag{2.5}$$

are the two time constants.

In addition density is a linear function of temperature and salinity, so

$$\rho = \rho_0[1 + \beta S - \alpha T] \tag{2.6}$$

and volume flux between basins is a linear function of density difference between basins, so

$$Q = C(\beta S - \alpha T). \tag{2.7}$$

The reason for multiple states is easily visualized by inspecting curves of density due to salinity and temperature and their sum as a function of Q. From (2.3) and (2.4) the first two curves are hyperbolas as shown in Fig. 2. Their sum can have positive and negative values for certain values of the parameters. For these plots a value of $\beta S^* = 0.0014$ was used and αT^* was assigned three different values. For small temperature forcing, the salt mode is too small to cause the sum to become negative. The straight line corresponding to Eq. (2.7) can intersect the curve in only one point

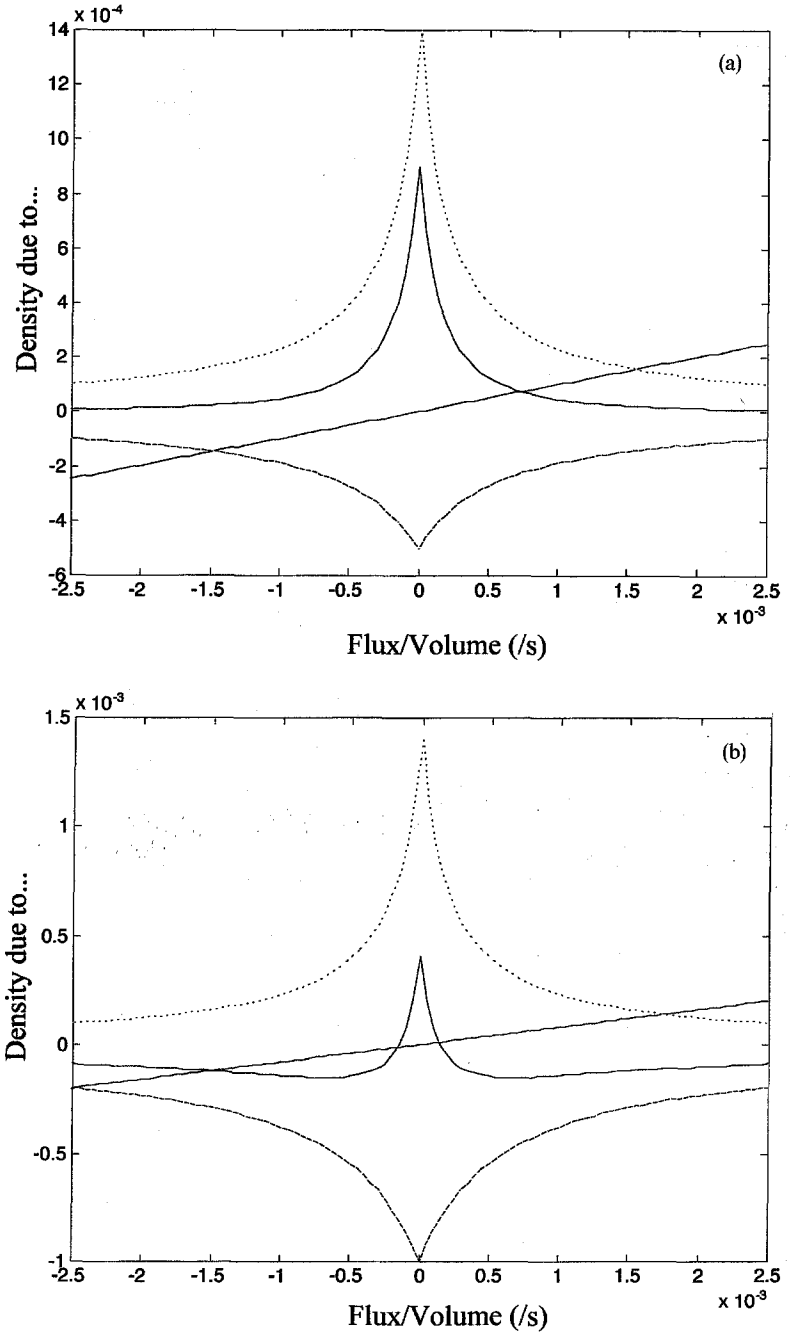

Fig. 2. Values of density due to salinity (dotted), temperature (dashed), and added together(solid) as functions of volume flux between the chamber and reservoir. Values relatively close to the experiment are used for these curves. Also shown is a typical straight line which corresponds to Couette flow through the pipe: (a) low thermal forcing $\alpha T^* = .0005$; (b) moderate thermal forcing $\alpha T^* = 0.001$; (c) strong thermal forcing $\alpha T^* = 0.0015$.

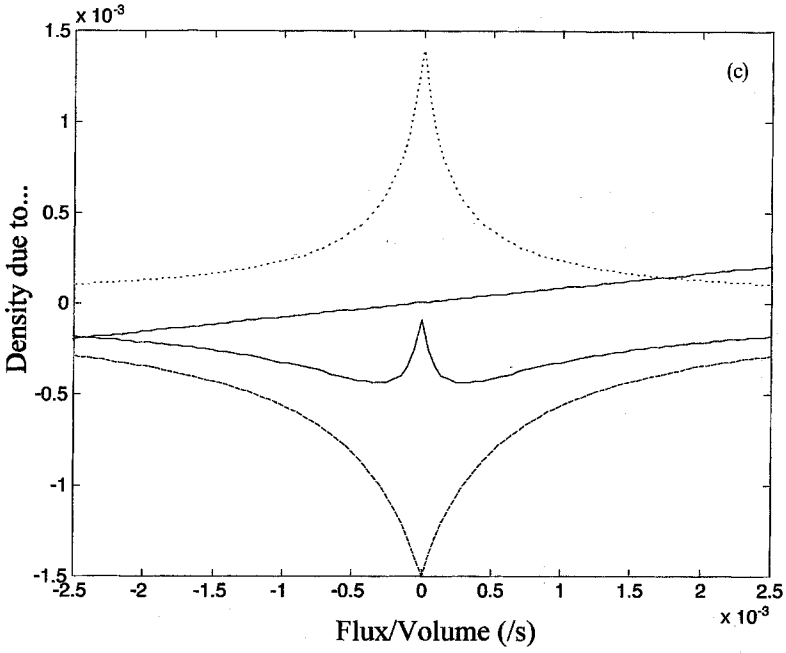

Fig. 2. (continued)

and that corresponds to the salt mode. For intermediate forcing, both positive and negative values are possible and the straight line corresponding to Eq. (2.7) can intersect the curves in three places. For large temperature forcing the sum is always negative and the line only intersects the curve at one point which corresponds to the thermal mode. The summed density can have positive and negative values of density within certain ranges of the forcing parameters. Using (2.7) one can see there are values of C that allow the straight line in Fig. 2 to intersect the density curves in more than one spot. Thus our experimental task was to set T^* and S^* to produce both values of density and to design a container with appropriate values of C.

To make sense of the experimental results, it was necessary to measure and calculate the change of density due to both salinity and temperature very accurately. Temperature data from two thermocouples (one in the chamber and one in the "ocean") and density data from an Anton Paar densiometer accurate to four significant figures were automatically recorded every 30 or 60 s for many hours which were the duration of each run. The effect of both temperature and of salinity to density difference between water in the chamber and in the "ocean" were then separately determined. The equation of state of seawater from [3] was used to calculate density difference between chamber and ocean due to temperature accurate to less than 0.0002 g/cm^3 for all cases. Density due to salinity was from the densiometer and accurate to better than 0.0002. Finally, the density of samples of the ocean water was measured after the experimental run and subtracted from the densiometer readings to determine density difference between chamber and ocean.

The results of these experiments verify the main predictions of the theoretical work. Fig. 3 shows the results of over two months of continuous runs. The volume flux and salinity of the steadily injected water was kept the same in every run, while temperature of the bath below the copper plate was systematically varied. Plotted are values of density due to temperature and salinity as a function of copper plate temperature.

Here is what the experiment revealed: For small bath temperatures, the density due to salinity is greater than density due to temperature, but only by a small amount. The chamber is in the salinity driven mode

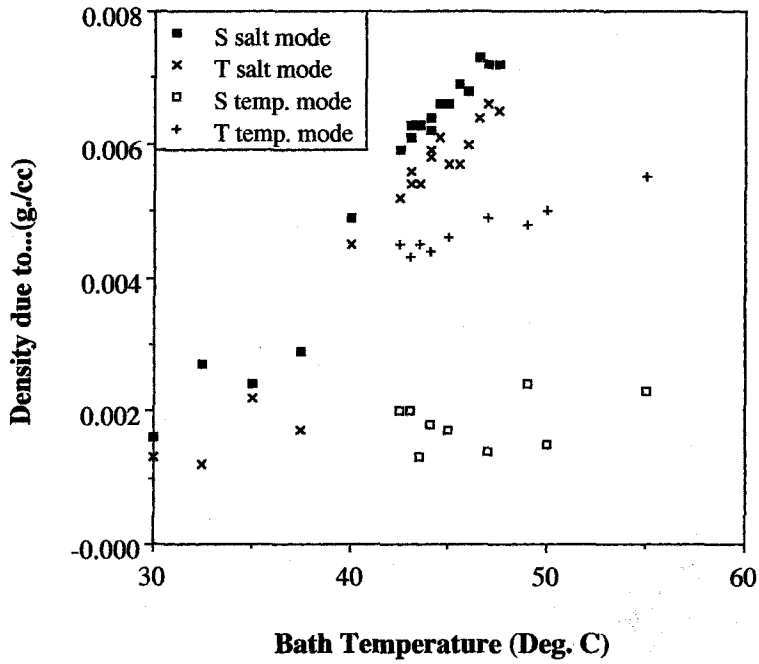

Fig. 3. Density due to temperature and salinity for the experimental test chamber sketched in Fig. 1. Each data point was taken after many hours of experimental run. These data were taken over many weeks of continuous running.

of flow. Fresh water entered through the top tube and left as warm and salty water through the bottom tube. This continued as the mode of motion for all runs up to a temperature of 42°, and as one of two possible mode for selected runs from there up to 48°. Above this value, the salinity driven mode was absent. From 42° upward there was a second state, shown as the lower pairs of data points. In this mode, density due to temperature was always much greater than density due to salinity. Fresh water entered through the bottom tube and left as hot and slightly salty water through the top tube. This state was the only state observed above 48°.

In the range where either state could exist there were some important features that show the dynamics of the flows that are driving the motion. First, the densities in the salinity driven mode are both higher than the densities in the temperature driven mode. Injection of dye in the tubes to see the flow revealed that the flow through the tubes was much slower in the salinity driven mode than in the temperature driven mode. This slow flow was produced because density due to salinity and temperature were close to the same value, with salinity just slightly greater. This slow flow also caused the large densities in the chamber. In the temperature driven mode, velocities were significantly faster (and of course opposite in sign) and density difference from temperature and salinity was much larger. Density due to salinity, which is the component with the slow thermal time constant, is small in the chamber because of the strong flushing whereas density due to temperature is greater density due to salt since temperature has roughly three times faster time constant.

3. Forced convection

Comparable processes can be found if stress driving replaces salinity driving. This fact is mentioned in an analysis of a loop model by Stommel and Rooth [10] yet the consequences to oceanography or in mechanics seem to be largely overlooked. Consider the case of a container of volume V containing water of temperature T connected to a large basin with two

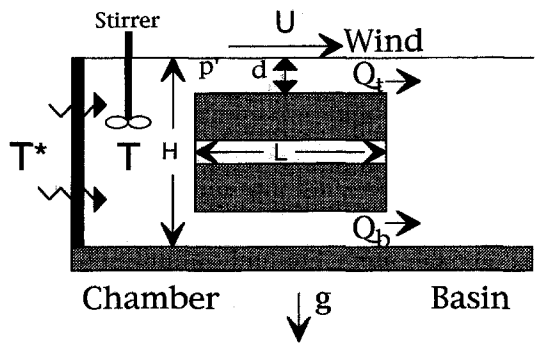

Fig. 4. Schematic of imaginary apparatus to produce multiple states with surface stress and heating.

rectangular channels, one at the top and one at the bottom as sketched in Fig. 4. The channels are of W width, d depth and L length. The container is in thermal contact with a bath at temperature T^* through a wall such that the thermal time constant of the container water is t. The flow in each channel obeys a viscous flow law

$$\frac{\partial p}{\partial x} = \mu \frac{\partial^2 u}{\partial z^2}, \tag{3.1}$$

where μ is viscosity, u is positive lateral velocity in the direction out of the container, z is the vertical direction and p is pressure in the container next to the beginning of each channel. The pressure is in deviation of pressure in a second large basin of zero temperature which lies at the outlet of the two channels. The top channel is exposed to a surface flow of magnitude U out of the channel. The volume flux out of the top channel using (3.1) is

$$Q_t = \frac{d^3 p' W}{12\mu L} + \frac{UdW}{2}, \tag{3.2}$$

where p' is pressure at the top of the container in deviation from pressure at the top of the outer basin. Pressure next to the bottom tube in deviation from pressure at the same depth in the outer basin is found by integrating the hydrostatic equation. This produces a volume flux out of the bottom channel which must be

$$Q_b = \frac{d^3 p' W}{12\mu L} - \frac{\rho g \alpha T H d^3 W}{12\mu L} \tag{3.3}$$

and since the sum of the flow out of both channels must be zero

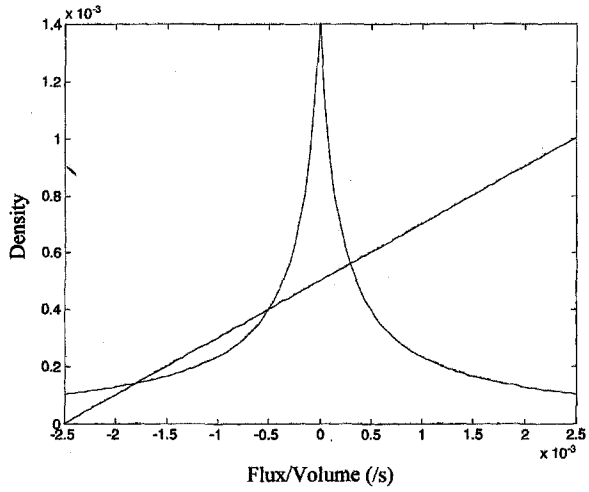

Fig. 5. Density due to thermal forcing (curves) and flow due to buoyancy driven motion in the presence of stress (straight line).

$$\frac{d^3 p'}{6\mu L} + \frac{Ud}{2} - \frac{\rho g \alpha T H d^3}{12\mu L} = 0, \tag{3.4}$$

so top volume flux is

$$Q_t = \frac{UdW}{4} + \frac{\rho g \alpha H d^3 T W}{12\mu L}. \tag{3.5}$$

For fixed negative U the relation between Q and T is shown in Fig. 5, which is similar to a figure in [10].

The heat balance in the container is

$$\frac{dT}{dt} = \frac{1}{\tau}[T^* - T] - \frac{|Q|T}{V}, \tag{3.6}$$

where volume flux can be either of the above expressions. For steady state

$$T = \frac{T^*}{1 + |Q|/V\tau}, \tag{3.7}$$

which is the hyperbola in Q, T space that is shown in Fig. 5. For the case drawn, the two trajectories intersect in three places. The two outside intersection points are stable solutions, the third is unstable and the system evolves to one of the other two states.

4. Forced convection in a shallow rotating basin

In an approach similar to that developed by Hansen and Rattray [4] for nonrotating flows and by Stommel and Leetmaa [11] for rotating flows, we assume there

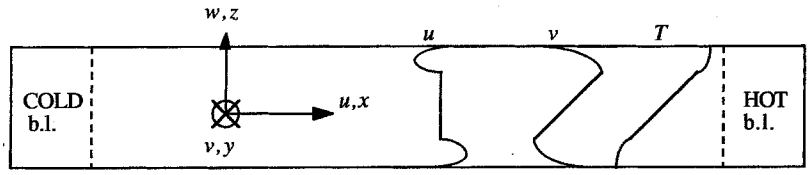

Fig. 6. Sketch of the model of the continental shelf and the vertical distribution of u, v, and T. The regions labeled "b.l." denote end regions where boundary layers involve vertical motions.

is an infinitely long and very wide continental shelf of uniform depth d with variation of temperature across its breadth (i.e. from coast to offshore) as sketched in Fig. 6. The system is rotating at rate $f = 2\Omega$ in gravity field g. The fluid has coefficient of thermal expansion α viscosity ν, and thermal diffusivity κ. It will be assumed that there is no variation in velocities and temperature deviation along or across the shelf direction, but that a uniform and steady flow is set up. A formulation was produced by the author [13] for a long shallow shelf of constant depth in a rotating fluid where the total temperature was expressed as

$$T' = (x + dT)\,\frac{\partial T_0}{\partial x}, \tag{4.1}$$

so it is composed of a uniform temperature gradient $\partial T_0/\partial x$ across the shelf (direction x) plus a deviation T that only varies in the vertical direction z. This formulation could yield analytical solutions for a number of physically interesting problems. Assuming that there is no variation in velocities along or across the shelf, using d as the vertical length scale and fd as the velocity scale, the following nondimensional equations apply:

$$-v = -\frac{\partial p}{\partial x} + E\frac{\partial^2 u}{\partial z^2}, \tag{4.2}$$

$$u = E\frac{\partial^2 v}{\partial z^2}, \tag{4.3}$$

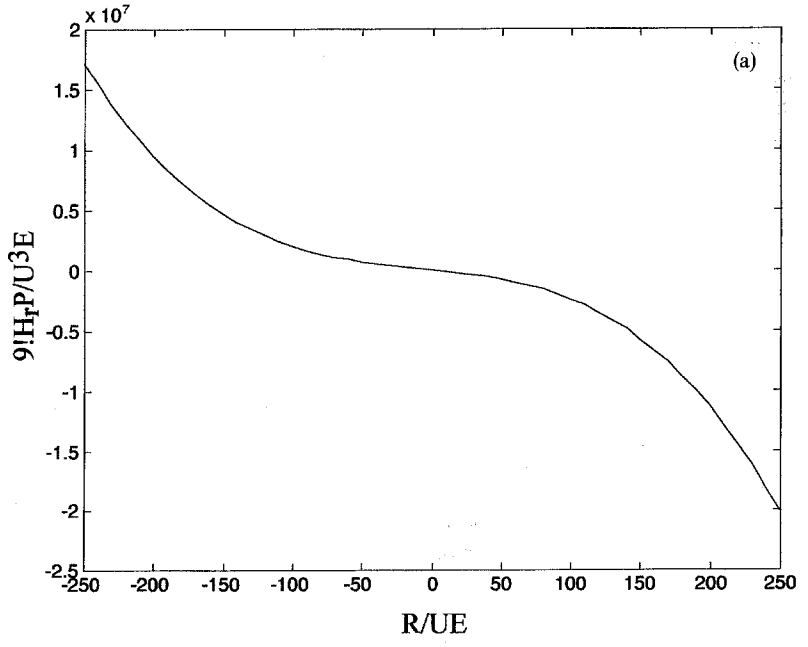

Fig. 7. Solutions of (a) Eq. (4.8), and (b) Eq. (4.9) showing a region where more than one value of R/U gives the same heat flux; (c) a close-up of (b).

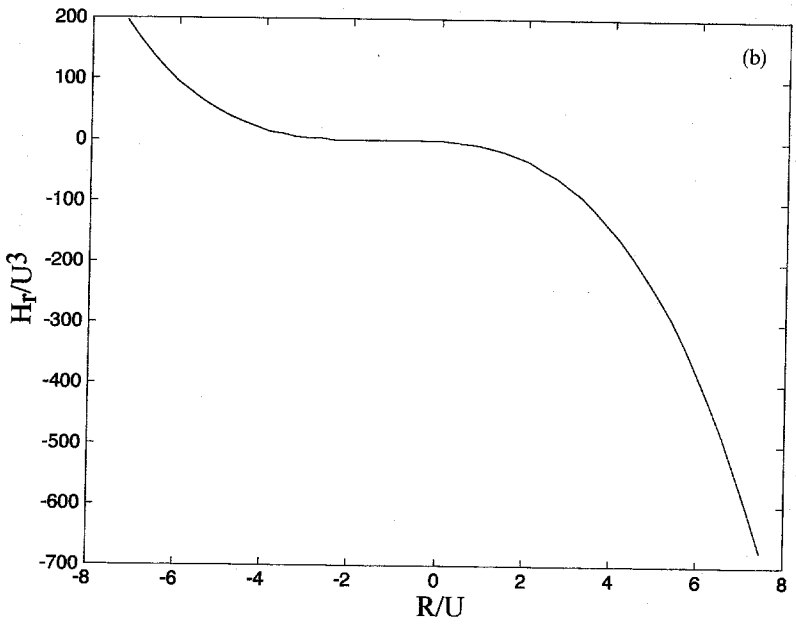

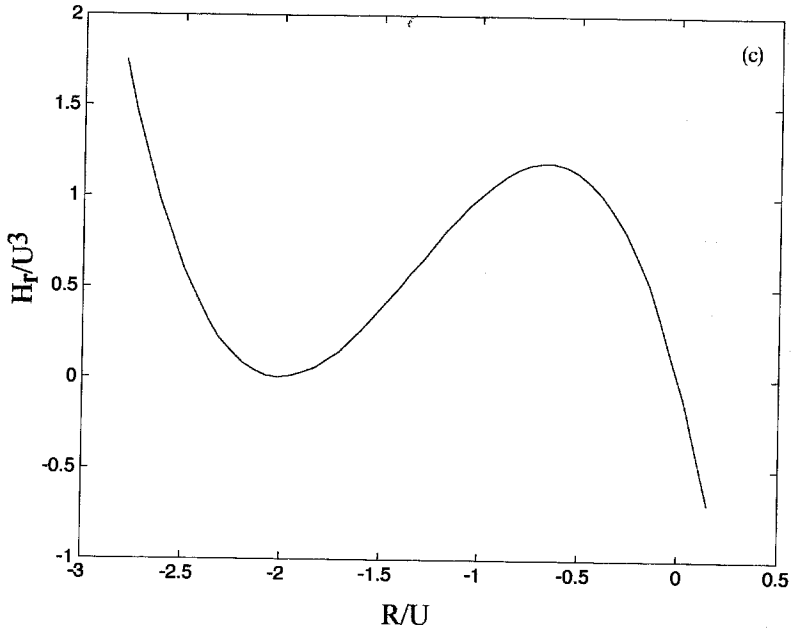

Fig. 7. (continued)

$$\frac{\partial p}{\partial z} = -Rx, \tag{4.4}$$

$$u = P\frac{\partial^2 T}{\partial z^2}, \tag{4.5}$$

where y is the along shelf direction and $R = g\alpha\partial T/f^2\partial x$, $P = \kappa/fd^2$, $E = \nu/fd^2$. Solutions with boundary conditions $u = \pm U$ and $\partial T/\partial z = 0$ at $z = \pm\frac{1}{2}$ (for simplicity) which correspond to motions

driven by both buoyancy and surface forcing were readily obtained. The equations are completely linear and assorted flows from different forcing or boundary conditions can be added together.

We could think of the heat transfer of such flows as that of a heat pipe (or more precisely a heat sheet) where heat is supplied in the warm region and transported laterally (downgradient) to the cold region. The transport mechanism is quite straightforward. A vertical temperature profile is produced through a balance between lateral advection and vertical diffusion using Eq. (4.5). The altered temperature is advected by velocity u one way near the top and the other way near the bottom. Of interest here is heat flux per unit shelf length. Of course this is not a linear function of R and U.

Expressions for heat flow have been worked out. For the case of large Ekman number the flow is viscous flow and the solutions can be represented as polynomials similar to those found by Hansen and Rattray. The dimensionless heat transport is

$$H = -\frac{R^2}{9!PE^2} - \frac{4!UR}{9!PE} - \frac{4!U^2}{6!P} \quad \text{for } E \gg 0.1. \tag{4.6}$$

For small Ekman number the flow possesses a thermal wind driven by the lateral temperature gradient in the interior and Ekman layers at the boundaries. The thermal wind transports no heat since it flows at right angles to the temperature gradient, but the flux in the Ekman layer does transport heat. Dimensionless heat transport is

$$H = -Pr\left(\tfrac{1}{2}R + U\right)^2 \quad \text{for } E \ll 0.01. \tag{4.7}$$

Since temperature is scaled using the lateral temperature gradient, H is defined using lateral temperature gradient as a scale. However, we seek a relation between temperature gradient and dimensional heat flux so it is necessary to remove the lateral temperature gradient from the heat flux scale. Rescaled heat flux obeys the relation

$$\frac{9!H_r}{U^3} = \frac{9!H_d g\alpha\kappa}{\rho C_p f^3 d^3 U^3} = -\frac{R}{U}\left[\frac{R^2}{U^2PE^2} + \frac{4!R}{UPE} + \frac{9!4!}{6!P}\right] \tag{4.8}$$

and

$$\frac{H_r}{U^3} = \frac{H_d g\alpha\kappa}{4\rho C_p f^3 d^3 U^3} = -\frac{R}{U}\left[\frac{R}{U} + 2\right]^2, \tag{4.9}$$

where H_d is dimensional heat flux with units of watts per meter of coastline, ρ is density, and C_p is specific heat. Note that R is proportional to lateral temperature gradient and U is proportional to the antisymmetric velocity imposed at the boundary. The relationship between R/U and heat flux for constant U is sketched in Fig. 7 for the cases of both large and small E.

The solution for large E exhibits a monotonic decrease of heat flux with R/U. But for small E there is a range (see Fig. 7(c)) where there is an increase of H_r with R/U. Let us investigate the behavior of this heat sheet if a set value of heat flux were imposed in this range, for instance by an electrical heater and let us assume that surface flux, or stress, is fixed. In the range three different negative values of lateral temperature gradient could remove that amount of heat. Given that U and $\partial T_0/\partial x$ are positive, the imposed velocity produces top fluid flowing from the cold end (left) toward the warm end on the right. This is opposite in direction to buoyant-driven convection, where top fluid flows from warm to cold. The flow with the greatest negative temperature gradient corresponds to interior flow taking place predominantly in the direction of convection. In this case the convection overpowers stress-driven flow and heat flux is produced by velocity in the Ekman layers that is predominantly produced by the thermal wind. The flow with the smallest absolute value of temperature gradient corresponds to predominantly stress-driven flow. That is to say, convection produced Ekman layer velocities (i.e. velocities that would happen in the absence of U) are weaker than stress driven (Couette) velocities. The stress driven flow drives flow in the Ekman layers that transports the heat, although it is hindered a little bit by buoyancy. The flow with the intermediate value of temperature gradient is unstable. For a given heat flux, if gradient were to slightly decrease in magnitude the heat flow would need to increase. But if heat flux is imposed, this increase is not possible, and the result is a decrease in temperature gradient which drives R/U toward the right. This process continues until the lowest of the three values

of R/U is approached. Likewise, if the absolute value of temperature gradient were to slightly increase, heat flow would decrease and $|R/U|$ would increase some more and finally the system would approach the greatest value of $|R/U|$. Thus the intermediate value is an unstable point the other two are stable points.

5. Concluding remarks

Although multiple solutions could exist for forced convection, there is need for caution as the effect of hydrodynamic instabilities has been neglected. The quantitative results given here may not apply in detail to many actual situations. If the stress driven flow predominates a density inversion is produced. For vertical convection cells not to exist, the Rayleigh number S/PE must be smaller than a critical value. Since E and P must be small, this requires that S be extremely small. In addition there is the possibility of baroclinic eddy transport that may play an important role in an actual system.

Acknowledgements

John Salzig constructed the apparatus and data gathering system. Support for this research was received from the Coastal, Polar, and Physical Oceanography Sections of the US Office of Naval Research under grant number N00014-89-J-1037.

References

[1] F. Busse, Das Stabilitatsverhalten der Zellular-konvektion bei endlicher Amplitude, Dissertation, University of Munich (1962) (translated from the German by S.H. Davis, the Rand Corporation, Santa Monica California, 1966).

[2] F. Busse, On the stability of two-dimensional convection in a layer heater from below, J. Math. Phys. 46 (1967) 140–149.

[3] N.P. Fofonoff and R.C. Millard, Jr., Algorithms for computation of fundamental properties of seawater, UNESCO Technical Papers in Marine Science No. 44 (1983).

[4] D.V. Hansen and M. Rattray, Gravitational circulation in straits and estuaries, J. Marine Res. 23 (1965) 104–122.

[5] G.R. Ierley and V.A. Sheremet, Multiple solutions and advection-dominated flows in the wind-driven circulation. Part I. Slip, J. Marine Res. 53 (1995) 703–737.

[6] S. Jiang, F. Jin and M. Ghil, Multiple equilibria, periodic, and aperiodic solutions in a wind-driven, double-gyre, shallow-water model, J. Phys. Ocean. 25 (1995) 764–786.

[7] W.V.R. Malkus and G. Veronis, Finite amplitude cellular convection, J. Fluid Mech. 4 (1958) 225–60.

[8] A. Schluter, D. Lortz and F. Busse, On the stability of steady finite amplitude convection, J. Fluid Mech. 23 (1965) 129–44.

[9] H. Stommel, Thermohaline convection with two stable regimes of flow, Tellus 13 (1961) 224–30.

[10] H. Stommel and C. Rooth, On the interaction of gravitational and dynamic forcing in simple circulation models, Deep-Sea Res. 15 (1968) 165–170.

[11] H. Stommel and A. Leetmaa, The circulation on the continental shelf, Proc. Natl. Acad. Sci. 69 (1972) 3380–3384.

[12] A.J. Weaver and T.M.C. Hughes, Stability and variability of the thermohaline circulation and its link to climate, Trends Phys. Ocean. 1 (1992) 15–70.

[13] J.A. Whitehead, Laboratory models of circulation in shallow seas, Phil. Trans. Roy. Soc. London A 302 (1981) 583–595.

[14] J. Marotzke, Ocean models in climate problems, in: Ocean Processes in Climate Dynamics: Global and Mediterranean Examples, ed. P. Malanotte-Rizzole and A.R. Robinson. (Dordrecht, Kluwer) pp. 79–109.

[15] J.A. Whitehead, Thermohaline ocean processes and models. Annu. Rev. Fluid Mech. 27 (1995) 89–113.